A New Multispectral Imaging System for Examining Paintings

Haida Liang,* David Saunders and John Cupitt
Scientific Department, The National Gallery, London, UNITED KINGDOM

A new multispectral system developed at the National Gallery is presented. The system is capable of measuring the spectral reflectance per pixel of a painting. These spectra are found to be almost as accurate as those recorded with a spectrophotometer; there is no need for any spectral reconstruction apart from a simple cubic interpolation between measured points. The procedure for recording spectra is described and the accuracy of the system is quantified. An example is presented of the use of the system to scan a painting of *St. Mary Magdalene* by Crivelli. The multispectral data are used in an attempt to identify some of the pigments found in the painting by comparison with a library of spectra obtained from reference pigments using the same system. In addition, it is shown that the multispectral data can be used to render a color image of the original under a chosen illuminant and that interband comparison can help to elucidate features of the painting, such as retouchings and underdrawing, that are not visible in trichromatic images.

Journal of Imaging Science and Technology 49: 551–562 (2005)

Introduction

It is now over a decade since the National Gallery in London developed the first multispectral imaging system to examine paintings. This system (VASARI) was based on a monochrome digital camera and a filter system that provided seven bands across the visible range (400 to 700 nm).[1] The resulting seven-band images produced extremely accurate colorimetric images of paintings for the National Gallery's long-term program of color monitoring,[2,3] but the multispectral data could not be used to derive convincing reconstructions of the reflectance spectra on a per pixel basis. Since the development of the VASARI system, the National Gallery has, like other research groups,[4,5] been aiming to develop multispectral imaging systems for paintings that have a higher spectral resolution. Reconstructing the reflectance data opens new possibilities, including more accurate comparison of color changes over time, the identification of pigments by comparison to standard libraries of reflectance spectra such as those held at the National Gallery, or available on the Internet,[6] and the simulation of the appearance of paintings after the removal of discolored or yellow varnishes. In addition, the recording of spectral rather than simple colorimetric data under a given illuminant will allow the colors in the painting to be rendered faithfully under any light source.

The EU-funded CRISATEL project, in which the National Gallery is a partner, has developed a multispectral camera with very high spatial resolution.[7,8] To model the performance of this large format camera during its development, a monochrome digital camera with a cooled CCD sensor and 14 bit electronics was used along with 13 interference filters. These filters cover the spectral range from 400 to 1000 nm, and have a bandwidth of 40 nm in the visible range and 100 nm in the near-infrared region (Fig. 1). Both the camera and the lights are mounted on an X–Y scanning stage such that the illumination and viewing geometry are fixed over the entire scan. The system is capable of scanning a 1 m^2 painting at 20 pixels per millimeter resolution in 20 minutes of total exposure time. This new system is different from the VASARI system in that the filters are between the detector and the lens rather than directly in front of the lights, more filters of narrower bandwidth are used, and the digital camera is more efficient. A detailed comparison of the two systems are given in the Discussion section. This article describes the calibration of the system, results from multispectral imaging of paintings and the application of the technique to the identification of certain pigments in paintings at the National Gallery.

System Characteristics and Calibration

The camera used in the system is a black and white Zeiss AxioCam normally used in microscopy. It has a Sony 1300 × 1030 cooled (30°C below ambient temperature) CCD sensor with a pixel size of 6.7 × 6.7 μm; it is capable of sampling at 3900 × 3090 pixels in micro-scanning mode. The lighting system consists of two identical

Original manuscript received October 11, 2004

Corresponding Author: H. Liang, Haida.Liang@ntu.ac.uk

*Current address: Physics and Mathematical Sciences, School of Biomedical and Natural Sciences, Nottingham Trent University, Clifton, Nottingham, NG11 8NS, UK

Supplemental Material—Figures 9, 10, 14, and 15 can be found in color on the IS&T website (www.imaging.org) for a period of no less than two years from the date of publication.

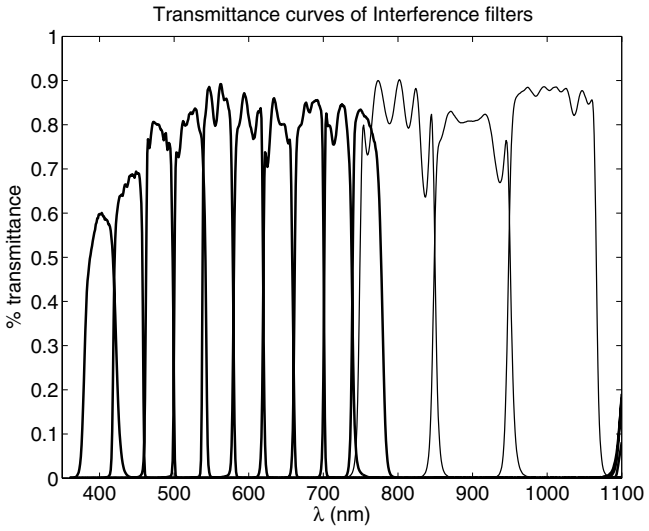

Figure 1. Measured visible and infrared filter responses.

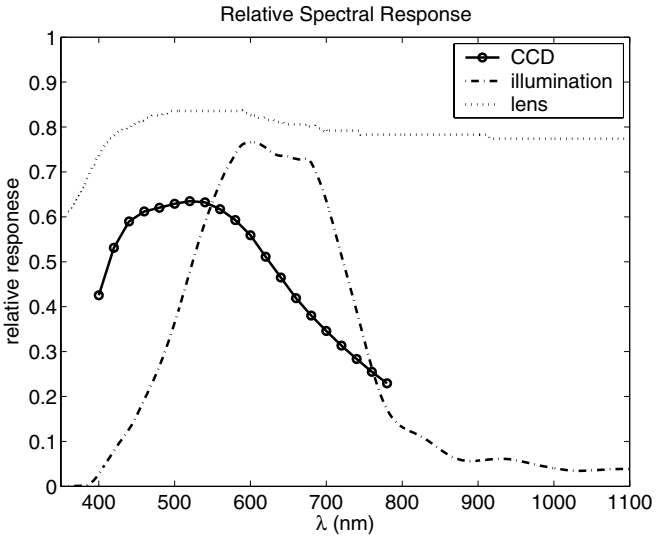

Figure 2. Spectral emittance of the lights, transmittance of lens, and sensitivity of CCD. The scale on the vertical axis is arbitrary.

82 V, 410 W tungsten lamps connected through optical fibers to six 'tails' that are evenly placed around the optical axis, illuminating the target at roughly 45°. A filter wheel that holds the 13 interference filters is placed between the detector and the lens. The transmittances of the filters were measured with a Hitachi U-4000 double beam spectrophotometer at sampling intervals of 2 nm (Fig 1). The lens is a Schneider Componon-S enlarging lens with a focal length of 80 mm. The camera needs to be refocused with each change of filter because of the variation in filter thickness. This is achieved by adjusting the lens focus. The closest object distance gives a resolution of 20 pixels per millimeter on the painting. An f-number of 5.6 was chosen to give the highest efficiency without vignetting and distortion. The transmittance of the lens provided by Schneider, the measured relative spectral sensitivity of the CCD, and the relative spectral emittance of the lights are shown in Fig. 2.

For the purpose of this study, the CCD was used at its lowest resolution, i.e., without micro-scanning. The response of the CCD was found to be linear over almost the entire range (Fig. 3), and the mean dark current was found to be constant with exposure time. Each series of a dozen dark frames was taken at the same exposure as the target frame, to produce master dark frames to be subtracted from target frames. Exposure times per channel were adjusted such that the frames are not saturated and the signal-to-noise ratio is the same for each channel when a perfect white target, i.e., 100% spectral reflectance across the channels, is imaged.

A white Teflon (PTFE) board was used for flat-fielding, and a Spectralon white from LabSphere was used as a white spectral target. An ideal flat-field frame compensates for both the inhomogeneity of the illumination and the variation in pixel-to-pixel response of the detector for each filter. However, these effects are normally coupled with the small scale inhomogeneity of the calibration target, unless the surface is perfectly smooth. A common way of separating the small scale inhomogeneity of the surface from the effects of illumination and detector response is by defocusing slightly.

We present here a robust and more accurate flat-fielding technique that avoids the need to defocus, and

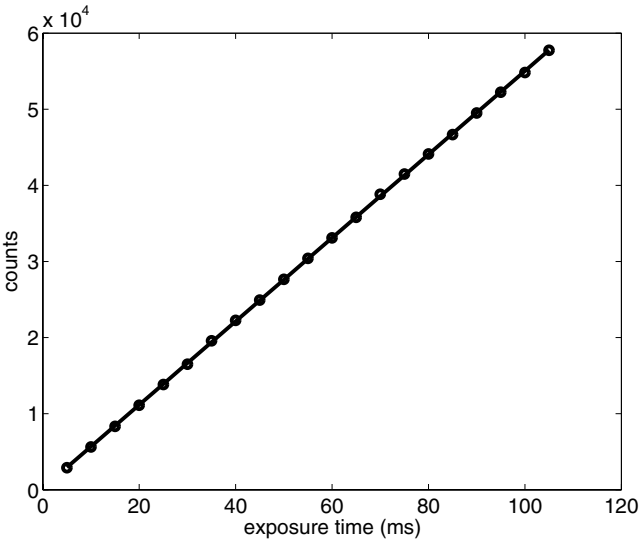

Figure 3. Median counts of images of a target versus exposure time: the circles are the measured median counts and the solid line is a straight line fit to the data.

has less strict requirements for surface smoothness and cleanliness of the white flat-field target. For each filter, a series of eleven images of the white Teflon board was taken at various random positions on the board (the white Teflon board should be larger than the camera field of view). The median image obtained, gives a true flat-field image that represents only the product of the lighting inhomogeneity and variation of the CCD pixel-to-pixel response; it is devoid of the small-scale inhomogeneities of the board. A normalized master flat-field produced for each filter in this way, was used to correct the target frames made with the same filter.

The central area of the dark-subtracted and flat-fielded image of the spectral white target was then used to calibrate the target frames spectrally.

Results

Spectral Reflectance

To check the accuracy of the measured spectra, we imaged two kinds of pigment based color chart: the Macbeth ColorChecker DC chart with 240 color and grayscale patches, and the PEBEO chart[7] with 117 color and gray patches duplicated in both a varnished (glossy) and an unvarnished version. A smaller version, the Macbeth ColorChecker chart, with only 24 color and gray patches was also used as a routine test chart. While the commercially available Macbeth ColorChecker DC chart is a pigment based chart with a wide color gamut, it was thought to be unrepresentative of the spectral reflectance of pigments found in old master paintings. A chart that is more representative of artists' pigments was developed in the CRISATEL project by PEBEO.

For camera systems designed to reproduce accurate color images of the original, there is a standard colorimetric measure of the quality of the system that gives an indication of the significance of a color difference to a human observer, namely a mean ΔE_{ab} or ΔE_{00} for a color chart.[9–12] A human observer can barely discern a color difference of $\Delta E_{00} \sim 1$. In the case of a multispectral system designed not only to reproduce accurate color but also accurate spectra, there is currently no equivalent standard parameter. So far the most common parameters used for the purpose are a combination of a mean ΔE and a mean rms spectral difference between the measured or reconstructed spectra and the 'standard' spectra of a color chart measured with a spectrophotometer (as was evident from papers presented in the multispectral imaging sessions of recent conferences such as PICS 2003 and CGIV 2004). Until better ways of characterizing multispectral systems are devised, we will use these two parameters to judge the quality of our current system. In particular, color difference will be expressed in terms of ΔE_{2000}^{D65} under D65 illumination[11] and viewed by a 1931 2° CIE standard observer,[11] and rms spectral differences will be calculated between 400 and 700 nm at 10 nm intervals unless otherwise specified.

Quality of Spectra

A simple cubic spline or piecewise cubic Hermite fit was found to be able to recover the spectral reflectance from multispectral images (see Fig. 4). The piecewise cubic Hermite fit will be used hereafter as, compared with a simple cubic spline fit, it was found to give a better result especially at the extremes of the spectra. One of the contributions to spectral errors is the large bandwidth of the filters. The nominal center of each channel may differ significantly from the effective center, if for example the filter response is strongly asymmetrical with respect to the nominal center. A simple weighted average center wavelength can be obtained for each band:

$$\lambda_m(n) = \frac{\int S_n(\lambda)\lambda d\lambda}{\int S_n(\lambda) d\lambda} \tag{1}$$

where $S_n(\lambda)$ is the relative system spectral response for filter n, i.e., multiplying the curves in Fig. 2 and one of the filter response curves in Fig. 1. Simulations of measurements of the Macbeth ColorChecker DC chart using the multispectral system (first 10 channels only) show that using λ_m as compared to the nominal centers λ_0 improves the spectral accuracy from a mean rms spectral error of 0.023 to 0.007 (maximum rms error from 0.10 to 0.02). However, the difference in color accuracy between using the two sets of center wavelengths is much smaller: mean ΔE_{2000}^{D65} of 0.99 as compared to 0.92 (maximum ΔE_{2000}^{D65} of 3.8 as compared to 3.2). We can also deduce the optimum set of central wavelengths λ_{opt} that gives the minimum average spectral rms error for each channel through simulated measurements of the Macbeth ColorChecker DC chart with the multispectral system. The simulations show that by using λ_{opt}, the mean rms spectral error is reduced to 0.005 and mean ΔE_{2000}^{D65} is reduced to 0.81. A simulation for the glossy PEBEO chart gave an identical set of optimum central wavelengths. Table I gives a summary of the simulation results in terms of mean spectral rms error calculated at the ten wavelengths and ΔE_{2000}^{D65} for the various choices of central wavelengths using the ColorChecker DC chart. Since the simulations show that choosing λ_m rather than λ_{opt} gave only minor differences

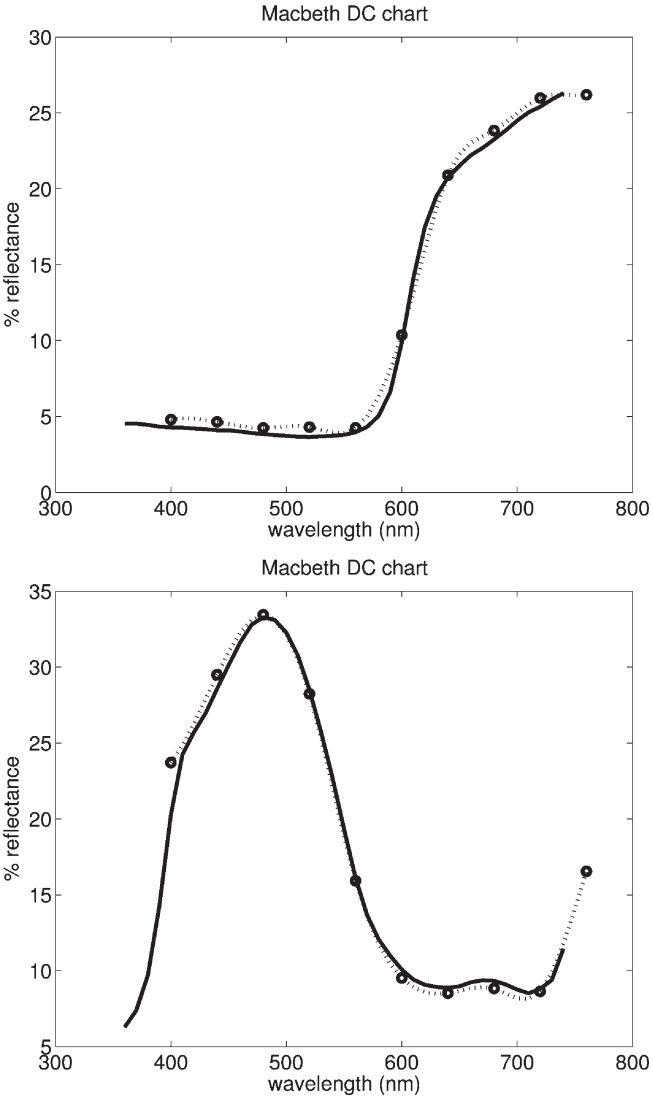

Figure 4. Two example spectra measured with the current multispectral system compared with those measured with a Minolta spectrophotometer. Spectra measured with the Minolta are shown as full lines, and the reconstructed spectra from a simple cubic spline interpolation between data points (circles) corresponding to each filter are shown as a dotted lines.

TABLE I. Spectral and Color Errors for Different Central Wavelengths from Simulated Data

Type	central wavelength										Spectral rms error	ΔE_{2000}^{D65}
λ_0	400	440	480	520	560	600	640	680	720	760	0.023	0.99
λ_m	415	443	482	525	559	599	640	680	718	756	0.007	0.92
λ_{opt}	412	444	485	523	561	600	638	680	721	752	0.005	0.81

TABLE II. Spectral Difference Compared with Minolta CM2600d Spectrophotometer

Chart	Raw Spectral rms diff. mean [max / min]	interpolated Spectral rms diff. mean [max / min]	$\Delta E^{D65}{}_{00}$ mean [max / min]
Macbeth	0.012 [0.051 / 0.002]	0.014 [0.043 / 0.001]	1.2 [3.7 / 0.2]
Macbeth DC	0.015 [0.064 / 0.003]	0.017 [0.061 / 0.003]	1.6 [7.4 / 0.4]
PEBEO (unvarnished)	0.014 [0.039 / 0.003]	0.016 [0.041 / 0.003]	1.9 [6.4 / 0.3]
PEBEO (gloss varnish)	0.015 [0.046 / 0.002]	0.017 [0.050 / 0.002]	1.8 [4.4 / 0.3]

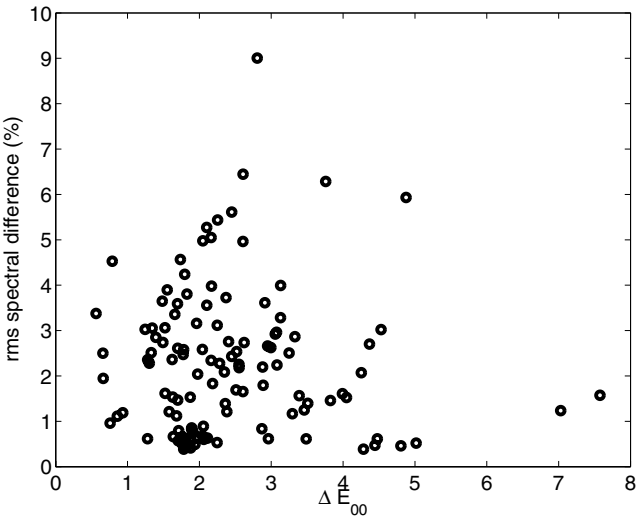

Figure 5. The rms spectral error per color patch on the glossy PEBEO chart is plotted against ΔE_{00}. There is no correlation between the two parameters.

in the mean rms spectral error and ΔE_{2000}^{D65}, λ_m will be used hereafter for generality. Table I shows that without taking into account any other sources of error, the mean rms spectral error for the ColorChecker DC chart would be 0.007 (ΔE_{2000}^{D65} of 0.92) using λ_m, as a result of the relatively broad bands and large spectral sampling steps of the multispectral system.

Table II summarizes the differences in terms of rms spectral differences and ΔE_{2000}^{D65} between the spectral reflectances obtained from the multispectral system and those from the Minolta CM2600d spectrophotometer for various test charts. The first column of Table II gives the raw rms spectral difference using data from the first eight filters before any interpolation; the second column gives the rms spectral difference after interpolation of the data in the spectral range 400 to 700 nm in steps of 10 nm. In this case, the Minolta measurements were made by collecting reflected light from a circular area of 3 mm in diameter, and the multispectral measurements were averaged over an area of 3.5×3.5 mm^2. It is important to note here that the spectra obtained from the multispectral system were simple cubic interpolations between the measured data, and were not reconstructed using any spectral reconstruction method, linear or nonlinear, which minimizes either the spectral difference or the ΔE between the reconstructed spectra and those of a spectrophotometer, for a standard color calibration chart. The differences listed in Table II include both intrinsic differences between the multispectral system and the Minolta spectrophotometer, random measurement errors and interpolation errors. Some of the intrinsic differences between the systems reflect a limitation in the multispectral system, for example, unlike a spectrophotometer, the multispectral system is an open system where each measurement area is affected by scattered light from its surroundings. On the other hand, the spectral and color differences resulting from the difference in illumination and viewing geometry between the systems, are not a limitation of the multispectral system. In other words, if we can find a spectrophotometer with the same illumination and viewing geometry as the multispectral system, then we will find that the spectral and color differences will be less than those listed in Table II.

To understand the relationship between color difference and rms spectral difference, the rms spectral difference for each color patch of a glossy PEBEO chart is plotted against the corresponding ΔE_{00} in Fig. 5. There appears to be no correlation between the two parameters. A small rms spectral difference does not necessarily imply a small ΔE_{00}, and a large ΔE_{00} does not necessarily imply a large rms spectral difference. The ultimate multispectral system is an imaging spectrophotometer which gives a small ΔE_{00} and accurate spectra (rms spectral difference is just one way of assessing spectral accuracy).

Figure 6 shows the color difference and rms spectral difference as a function of CIE L, a and b values for the glossy PEBEO chart. There appears to be no bias in color or spectral accuracy with respect to the color of a patch. However, as expected, there is an increase in ΔE values for the darkest patches (low L values) and a slight increase in rms spectral differences for the brightest patches. Figure 7 shows the median absolute spectral error as a function of wavelength for the glossy PEBEO chart. The spectral errors for the first ten filters roughly follow the shape of the median spectrum of the entire chart indicating that the fractional spectral error is roughly constant as a function of the wavelength.

Stability of the System

The stability of the instrument is important for the purpose of spectral/color monitoring. A small Macbeth

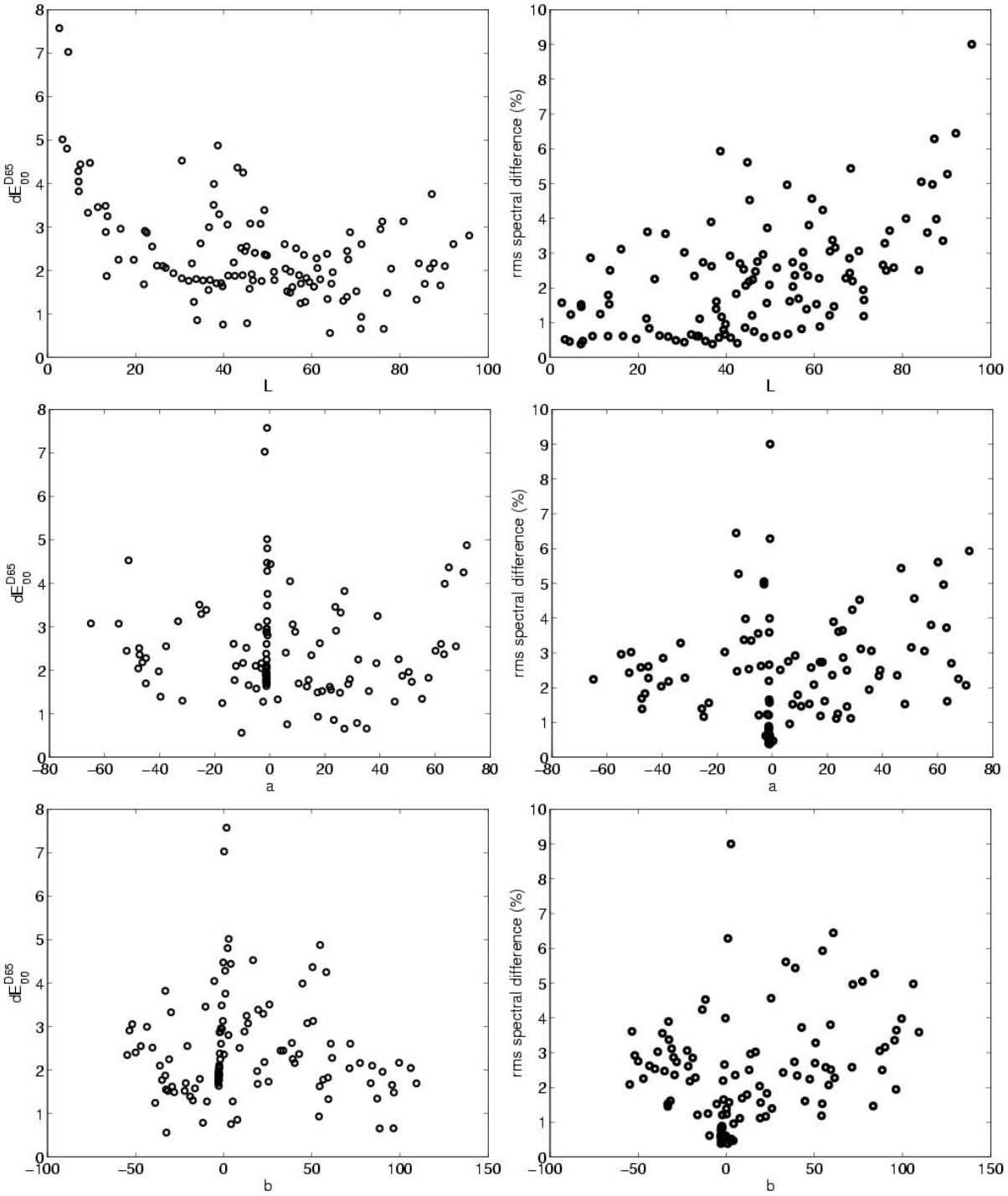

Figure 6. The left column shows the color difference ΔE_{00} as a function of the CIE Lab color terms; the right column shows the rms spectral difference (in percentage units) as a function of the CIE Lab color terms for the PEBEO chart with glossy varnish.

chart of 24 color and gray patches was used to check the stability of the system over three independent experiments at six monthly intervals. The relative spectral/color difference between the first and third, and the second and third measurements are shown in Table III. The color differences are presented in both ΔE_{ab}^{D65} and ΔE_{2000}^{D65} units. The color difference between any two independent measurements was found to be visually

TABLE III. Stability of Spectral Measurements

Exp.	Spectral rms diff. mean [min–max]	ΔE_{2000}^{D65} mean	ΔE_{ab} mean
1 – 3	0.011 [0.001–0.026]	0.91	1.3
2 – 3	0.013 [0.001–0.028]	0.96	1.2

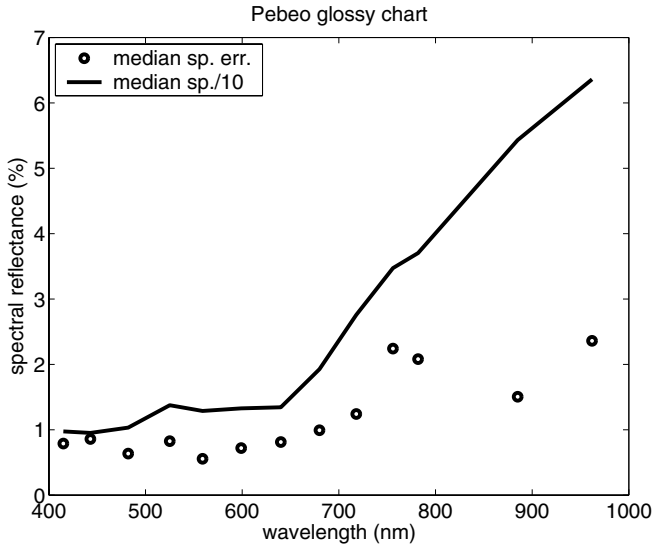

Figure 7. The median absolute spectral differences of the values measured for the 13 channels compared to those measured with an Ocean Optics spectrometer for the PEBEO chart with glossy varnish (shown as circles); for comparison the median spectra of the chart scaled by a factor of 10 is shown as a solid line.

insignificant to a human observer, i.e., the multispectral system is sufficiently accurate for the purpose of monitoring color or spectral changes. The absolute spectral/color accuracy is more difficult to establish, since spectral reflectance and color depend amongst other things on the illumination and viewing geometry. However, we can estimate the effect of geometry on spectral reflectance.

Effect of Geometry on Spectral Reflectance

We can compare the effect of illumination and viewing geometry on the spectral reflectance using a Minolta CM 2600d spectrophotometer with a diffuse/8° geometry (excluding specular reflection) and an Ocean Optics HR2000 fiber optic spectrophotometer fitted with a 45°/0° adaptor (see Fig. 8). Since the effect of geometry on spectral reflectance depends on the surface roughness and isotropy of the sample, we chose for comparison an example of a smooth painted surface, the PEBEO chart with a glossy varnish, and an example of a rough painted surface, a set of four charts of historic artists' pigments painted by hand (27 yellow patches, 28 red patches, 28 blue patches and 27 green patches). Table IV shows the difference in spectral reflectance measured by the two spectrophotometers for color charts of varying surface roughness for the spectral range of 400 to 700 nm. As expected, a difference in geometry produces a greater difference in spectral reflectance for rough painted surfaces compared with smooth surfaces. Even though the illumination and viewing geometry of the multispectral system is different from both systems shown here, Table IV gives an indication of the magnitude of the effect of geometry on the spectral reflectance measured. The mean rms spectral difference between the multispectral system and the Minolta spectrophotometer (see Table II) is comparable to the spectral difference caused by effects of geometry (see Table IV).

TABLE IV. Effect of Geometry on Spectral Reflectance

Chart	Spectral rms diff. mean [max / min]	ΔE_{ab} mean [max / min]	number of color patches
PEBEO (glossy)	0.012 [0.051 / 0.001]	1.4 [4.5 / 0.3]	117
Yellow	0.020 [0.053 / 0.006]	2.2 [6.7 / 0.6]	27
Red	0.019 [0.110 / 0.005]	2.5 [7.9 / 0.6]	28
Green	0.020 [0.062 / 0.006]	3.1 [9.6 / 0.9]	27
Blue	0.017 [0.034 / 0.004]	3.0 [9.0 / 0.4]	28

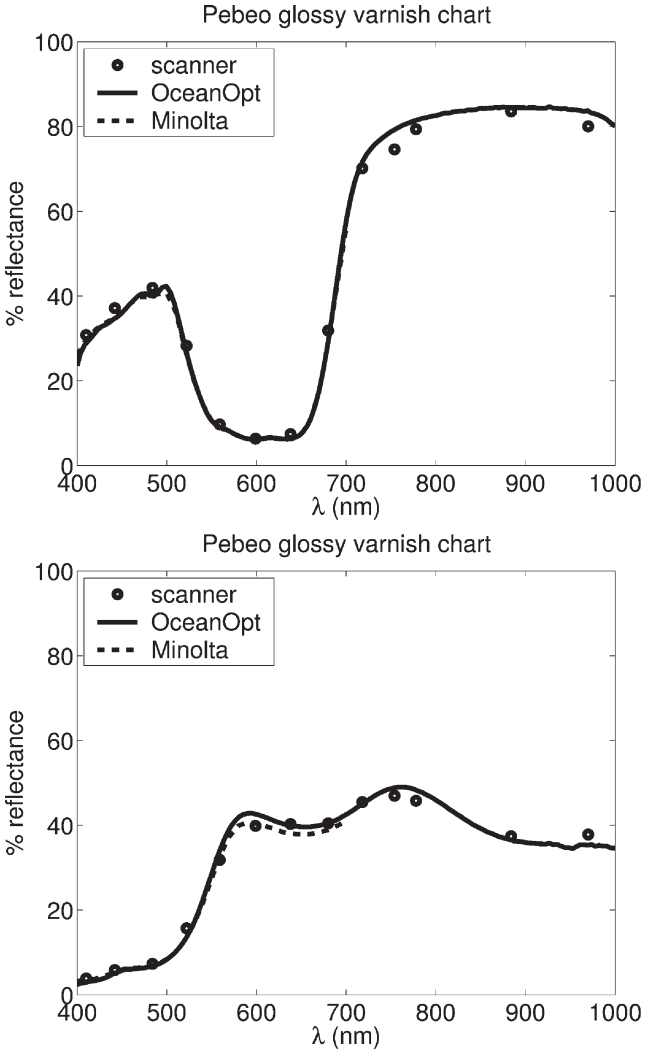

Figure 8. Two spectra from the glossy PEBEO chart obtained from the multispectral system (circles) compared with measurements made with the Minolta (dashed line) and Ocean Optics spectrometers (solid line): upper spectra, cobalt blue; lower spectra, yellow ochre.

Figure 9. An image under illuminant D50 of a painting by Crivelli (NG 907.2) rendered from the multispectral image. (Reproduced by permission of the Trustees of the National Gallery, London.) *Supplemental Material—Figure 9 can be found in color on the IS&T website (www.imaging.org) for a period of no less than two years from the date of publication.*

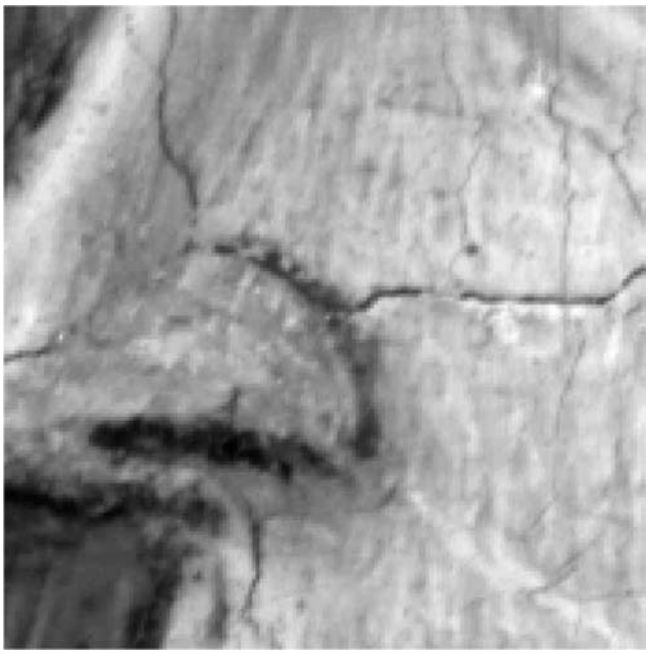

Figure 10. A high resolution detail showing the craquelure in the painting. *Supplemental Material—Figure 10 can be found in color on the IS&T website (www.imaging.org) for a period of no less than two years from the date of publication.*

Any spectral reconstruction method relying on knowing the 'true' spectral reflectance of a color chart, would be limited by the spectral difference caused by the difference in geometry between the multispectral system and the spectrophotometer used to measure the color chart.

Image Rendering

The system was next used to image paintings in the National Gallery Collection, providing per-pixel spectral information that allows the color appearance of the same painting under different illuminants to be simulated. The example given here derives from the data collected by the multispectral system for a painting of *St. Mary Magdalene* by the Venetian artist Carlo Crivelli [National Gallery, London, No. 907.2]. The painting was scanned in 32 individual images per filter, each 1300 × 1030 pixels in size, with an overlap between successive images of 100 pixels. At this imaging distance, the change in image scale between filters was less than 1 pixel. Hence, it was not necessary to resample the images onto the same scale. The corresponding images through different filters were aligned automatically using a cross-correlation routine in VIPS,[13] and the 32 images thus aligned were mosaicked together automatically for one reference channel; the other channels were then mosaicked in exactly the same fashion as the reference channel using the automatic mosaic routines in VIPS.

The spectral reflectance for each pixel obtained though a cubic interpolation between the 13 data points from 400 to 1000 nm, was then multiplied by the spectral power distribution of the chosen illuminant and the results rendered using the 1931 2° CIE standard observer weighting functions to give a color image of the painting under a specific illuminant. Figure 9, (*available in color on the IS&T website* (*ww.imaging.org*) *for a period of no less than two years from the date of publication*) shows a rendered color image of the painting under illuminant D50. An enlarged detail showing some craquelure is also shown in Fig. 10, (*available in color on the IS&T website* (*www.imaging.org*) *for a period of no less than two years from the date of publication*) to demonstrate that the image registration between the channels was accurate, since no color fringing was seen at the edge of the cracks.

For quality control, a small Macbeth chart of 24 patches was scanned at the same time as the painting,

TABLE V. Spectral and Color Errors for Different Filter Types

Type	spectral rms error mean (max)	ΔE_{2000}^{D65} mean (max)
CRISATEL	1.12 (2.77)	0.35 (1.11)
Square	1.14 (2.71)	0.34 (0.97)
Gaussian	1.45 (3.79)	0.56 (1.50)

and the spectral differences, compared with those measured with the Minolta CM 2600d, are listed in Table II (first line).

Discussion

The current multispectral system has a number of advantages compared with the old VASARI system. Apart from the improved camera sensitivity as a result of advances in CCD and camera technology over the last 10 years, we have also increased the number of filters from seven to ten in the visible and added three infrared filters. A fundamental difference between the two systems is that the filters are placed in the reflected light path (between the detector and the lens) in the current system instead of the incident light path (right in front of the lights). Filters placed between the detector and the lens change focus positions of the optical system depending on the thickness of a filter which can result in changes in image scale between channels, and any tiny misalignment of a filter could cause a significant shift in image position between channels. In the current system with a working distance of 0.5 m, the focus adjustment between filters does not result in a noticeable scale change, i.e., changes are less than a pixel, however, translations in image positions up to 19 pixels between channels were observed (a tilt of a fraction of a degree in the filter alignment can cause such a shift). A computer program using cross-correlation techniques was implemented to align the images automatically and efficiently. The VASARI system was originally designed to have the filters placed in front of the lights to avoid image scaling problems. Advance in processing speed of computers over the last 10 years means that such image scaling can now be achieved efficiently, hence image translation and scaling no longer pose a problem. In the VASARI system, the filters were placed in the lighting compartment and the heat from the lights could potentially alter the filter response. Another disadvantage of having the filters in the incident light path would be the inability of the system to distinguish the reflected light from light emitted at a different wavelength, e.g., in the case of fluorescence, making the system less robust.

The seven VASARI filters have their peak transmittance ranging from 400 to 700 nm in steps of 50 nm with roughly Gaussian spectral transmittance of 70 nm bandwidth. In comparison, the ten CRISATEL filters in the visible span the range 400 to 760 nm in steps of 40 nm with roughly square spectral transmittance of 40 nm bandwidth. The CRISATEL filters have higher peak transmittance (60 to 90%) compared with the VASARI set (60 to 70%). There was considerable overlap between the filters in the VASARI filter set, but minimal overlap in the CRISATEL filter set. There have been a number of studies conducted over issues of filter selection, e.g., Hardeberg IN 2003[14] and references therein. Here we will address issues of whether Gaussian spectral shape filters are preferable to square shape and whether overlapping filters are preferable to non-overlapping filter sets through simple simulations where we assume the filters to have the same bandwidth and peak response, the overall system is ideal with no noise, and that the spectral response of the system (excluding the filters) is flat. Table V shows simulated measurements of the Macbeth Colorchecker DC chart using a system with three different filter types: the first ten CRISATEL filters (see Fig. 1), and filters with square or Gaussian shaped spectral transmittances with 40 nm bandwidth in the range 400 to 760 nm at 40 nm intervals, i.e., ten filters in each case. The rms spectral errors were calculated from the interpolated spectra at 10 nm intervals. Central wavelengths of the filters were used for the simulated measurements. Both the mean and maximum rms spectral errors and the ΔE values indicate that square filters perform better than Gaussian. CRISATEL filters have spectral transmittances close to square shapes, hence the values are close to those of square filters.

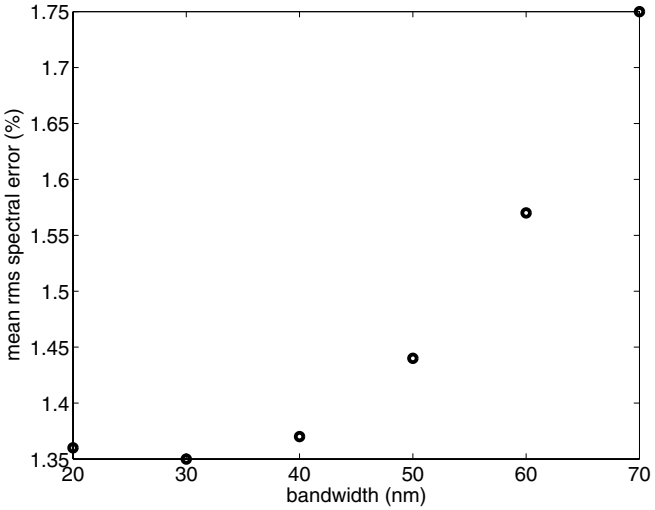

Figure 11. Simulated measurements of the Macbeth Colochecker DC chart using a system with 10 filters (squared shaped spectral transmittance) in the range 400 to 760 nm at 40 nm sampling interval. The system response excluding the filters is assumed to be flat as a function of wavelength. The mean rms spectral error is plotted against the bandwidth of the filters.

Any discussion on whether it is better to have overlapping filters or non-overlapping filters has to be well defined, since clearly a large number of non-overlapping narrow band filters is preferred to three wide band overlapping filters, and similarly a large number of overlapping narrow band filters is preferred to three non-overlapping filters. In practice, cost is the limiting factor, and cost usually limits the number of filters. Hence, we address the problem by fixing the number of filters to ten, centered between 400 and 760 nm at 40 nm intervals. The bandwidth is then varied to produce different levels of overlap, that is wavelength accuracy of a measurement is traded for overlaps in the filter response so as not to miss important spectral features. Square spectral shaped filters are used in the simulations. Figure 11 shows the mean rms spectral error plotted as a function of filter bandwidth from simulated measurements of the Macbeth ColorChecker DC chart using sets of filters with varying bandwidth. The rms spectral errors were calculated from the interpolated spectra at 10 nm intervals between 400 and 760 nm. It

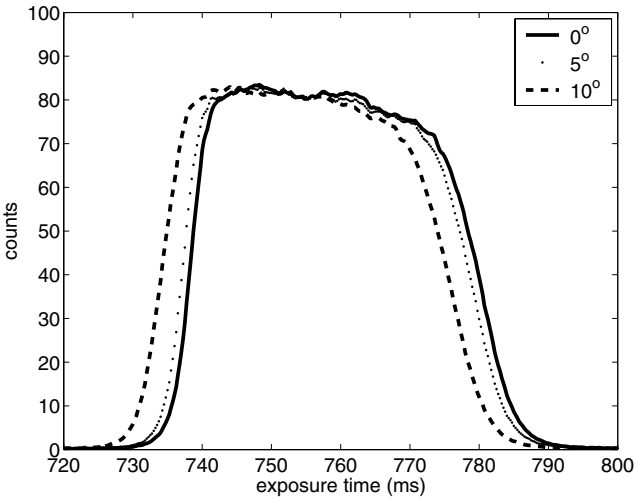

Figure 12. The transmittance curve through the 760 nm filter with incident angles of 0°, 5° and 10°.

shows that filters with bandwidth less than 40 nm, i.e., non-overlapping filters, are preferred in the case where the filter number is fixed to ten. This result is not surprising because spectra reflectance of pigments are very smooth. There is also little difference between a filter set of 20 nm bandwidth compared with 40 nm, which means that 40 nm bandwidth is the optimum in a real system since a wider band gives a higher throughput.

One of the characteristics of interference filters is that their transmittance spectra shifts as the angle of incidence changes. This could be a concern when used in wide angle multispectral systems. The field of view of the current system is ~ 8° which means the maximum angle of incidence is ~ 4°. The transmittance spectra measured for one of the CRISATEL filters for different angles of incidence is shown in Fig. 12, (*available in color on the IS&T website* (*www.imaging.org*) *for a period of no less than two years from the date of publication*). A tilt of 5° would result in a spectral shift of less than 2 nm (c.f. 40 nm bandwidth) with no noticeable change in spectral shape. Hence, in the case of our current system, the angular dependence of the spectral response of interference filters is not a concern.

The main JumboScan camera developed in the CRISATEL project uses the same filter set but it scans the painting in one sweep per filter and does not require mosaicking: it is also more portable than the multispectral system described here. One main difference between the two systems is that for the JumboScan the illumination and viewing geometry changes as it sweeps, which could potentially introduce color bias between the edge and the center of an image, whereas for the system described here the illumination and viewing geometry is fixed as it scans. The Thomson CCD line-array used in JumboScan has a lower sensitiviy (especially in the blue) compared with the Sony CCD in AxioCam used in this system. The lighting used in JumboScan is HQI rather than Tungsten halogen which means less spectral accuracy because of the emission lines.

Hyperspectral imaging systems that use tunable filters or dispersive systems such as diffraction gratings would give higher wavelength accuracy, but these systems are in general very slow and require huge data storage space. In the case of a liquid crystal tunable filter, the peak transmittance of the filter decreases as the wavelength decreases resulting in very poor blue response since the response of the CCD and emission of the lights are in general also low in the blue region.

We have shown that it is possible to treat a multispectral system with 10 filters in the visible region as an imaging spectrophotometer. The calibration procedure adopted here is close to that used for spectrophotometers, namely the spectral response is calibrated by a standard white target, e.g., LabSphere, and the wavelength is calibrated through measurements of the spectral transmittance of the filters along with the spectral variation in sensitivity of the rest of the system. There is no need to use a color calibration chart, unlike the case of broad band color imaging. For a multispectral system of the type described here, the sampling interval and bandwidth of the channels are either narrower or of the order of most of the narrowest spectral features in pigment reflectance spectra.

Applications

Pigment Identification

Generally, pigment identification using visible spectra is not a particularly efficient method; the observed surface color often gives as much information as the spectra themselves. In addition, a simple visual inspection of the surface of the painting under a binocular microscope can reveal particle size and shape, two characteristics that greatly assist pigment recognition. However, the addition of the three infrared channels may aid the identification of pigments through spectral reflectance, as the behavior of the pigments in the near infrared region is not evident in their color. A comparison of the reconstructed spectra with those measured with either spectrophotometer for the PEBEO chart and the Macbeth ColorChecker DC chart, shows that the new multispectral system is on the whole comparable to a spectrophotometer. This is not surprising, since the spectral reflectance curves of most pigments are smooth and only a few pigments, like cobalt blue and the red 'lakes', have fine spectral features on the 10–20 nm scale (see the spectra of cobalt blue in Fig. 8). The advantage of the multispectral system compared with a spectrophotometer is the greatly improved efficiency.

To assess the ability of the multispectral system to produce tentative pigment identifications, four regions were selected from the painting of *St. Mary Magdalene*. These regions were the bright red of her cloak, the green lining of the cloak, the blue fabric of her robe, and the purple–red brocade on the sleeve. For each color, the final averaged spectra were obtained from two separate regions, each comprising around 5,000 pixels (3.5×3.5 mm^2). These spectra were then compared with a spectral library of 63 historic artists' pigments to find the best match. The logarithm of the absorption and scattering ratio, log(K=S), as well as the spectral reflectance were used for the comparison. The log(K = S) parameter is more invariant to changes in concentration (a constant shift in the Y–axis) compared with either K=S or the spectral reflectance.[15] This is expected from the Kubelka–Munk model, and is experimentally verified as can be seen in the case of azurite in Fig. 13.

The blue pigment best matched the spectra of either azurite or Prussian blue mixed with white in the visible range. Under the binocular microscope these two pigments are easily distinguished: the mineral azurite (present here) has large angular particles, while

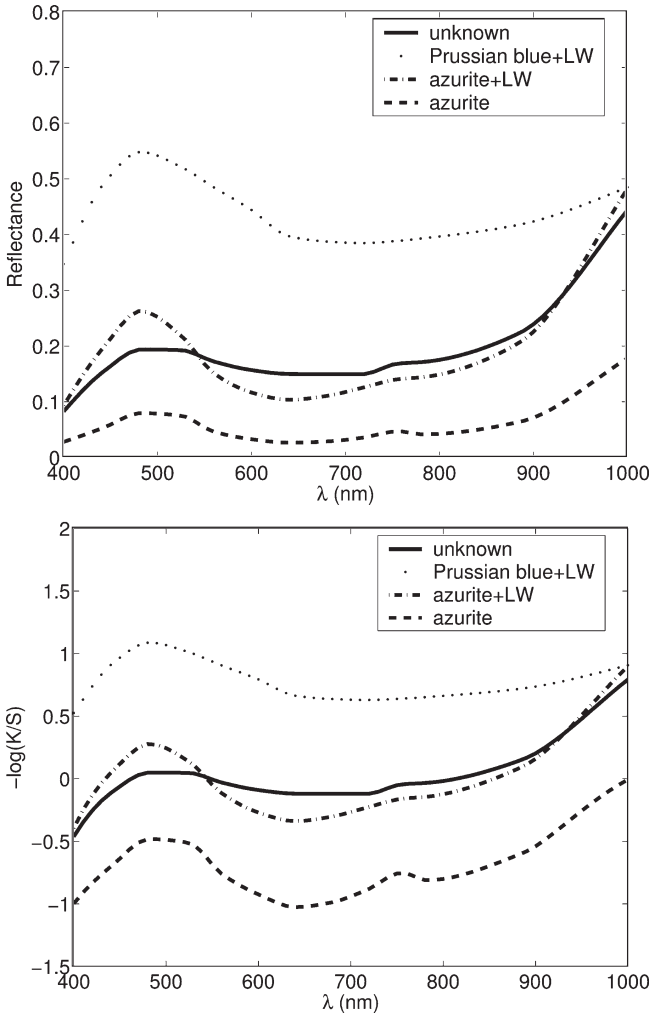

Figure 13. The best match for the blue pigment in the Crivelli painting NG 907.2. The upper figure shows the spectral reflectance curves and the lower figure shows the –log(K = S) curves. The solid black curve shows the measured spectrum from the blue region on the painting and the dotted curve shows the spectrum of a Prussian blue mixed with lead white, the dashed curve shows a pure azurite, the dot–dashed curve shows an azurite mixed with lead white, also measured with the multispectral system.

Prussian blue has much smaller, intensely colored particles. However, with the addition of the three infrared channels, the spectral method can also easily distinguish between the two pigments, since Prussian blue has a much lower relative spectral reflectance in the infrared compared with azurite. In this case, spectral matching gives azurite as the best match. Figure 13 shows the reflectance and –log(K=S) spectra of the blue region from the painting, and library spectra for azurite and Prussian blue from the library (both derived from spectral measurements obtained from the multispectral system). It is interesting to note that the spectrum from the painting shows a higher reflectance in the red and green regions than the library spectrum for pure azurite. Examination of a fragment of paint from the blue robe revealed high quality azurite mixed with small quantities of pale, yellowish green and red impurities (Fig. 14 *available in color on the IS&T website* (*www.imaging.org*) *for a period of no less than two years from the date of publication*).

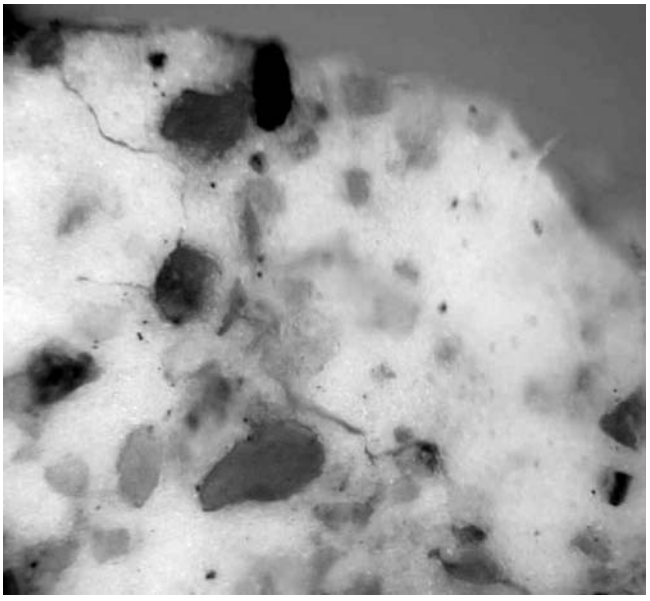

Figure 14. Photomicrograph of a tiny sample from the blue region of the robe in the painting (see Fig. 9). *Supplemental Material—Figure 14 can be found in color on the IS&T website (www.imaging.org) for a period of no less than two years from the date of publication.*

The bright red cloak provided a spectrum that best matched the traditional red pigment vermillion. The quality of the match was improved by the addition of a black pigment using a Kubelka–Munk method of mixture.[16,17] Again, an examination of a sample taken from the painting showed that the modeling in the cloak had been achieved using thin lines of black paint over a body color of vermillion (Fig. 15 *available in color on the IS&T website* (*www.imaging.org*) *for a period of no less than two years from the date of publication*). The green paint gave good matches for verdigris, Scheele's green, and emerald green mixed with white. As emerald and Scheele's green were synthesised in the early 19th and late 18th century respectively, the limitations of spectral matching are again emphasised. Other analytical methods would again be required to establish the nature of the pigment. The red brocade on the sleeve was consistent with the spectra of red lake pigments, although it was not possible to be more specific as the spectra of these lakes vary with method of preparation and are broadly very similar.

Interband Comparisons

Interesting comparisons can be made between the images captured at different wavebands. The near infrared channels of the system correspond to the spectral range traditionally used for infrared photography. Infrared photography has been used for at least 60 years[18,19] to study the condition of paintings and for revealing signatures and underdrawings underneath paint layers in old master paintings. However, the sensitivities of the films used in infrared photography are low compared with modern digital technology.

In the example shown here, the infrared image captured by the multispectral system at 900 nm clearly shows the underdrawing on the palm of the hand, which

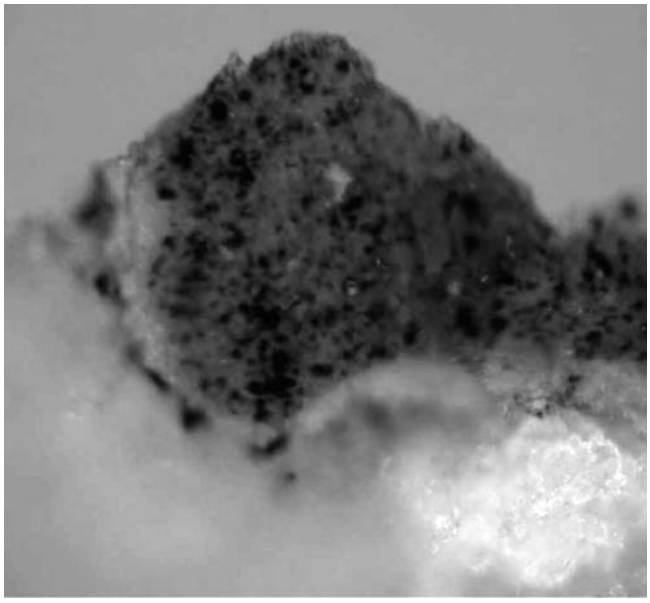

Figure 15. Photomicrograph of a tiny sample from the red area of the cloak in Fig. 9. *Supplemental Material—Figure 15 can be found in color on the IS&T website (www.imaging.org) for a period of no less than two years from the date of publication.*

is not seen in the 560 nm image (Fig. 16). Similarly, the 900 nm image reveals a number of circular areas on the wall around the hand which are old damages that have been repaired by a conservator. The color of these retouchings was well matched to the original paint in the surroundings, so that it is not easily discernable under visible light (see Fig. 9). However, the spectral reflectances of the retouchings and the original paint are clearly different in the infrared. Figure 17 shows a detail around the right foot in the 13 bands and the rendered color image, which shows that the retouchings and defects that were not visible in the color image were revealed in the red and infrared images.

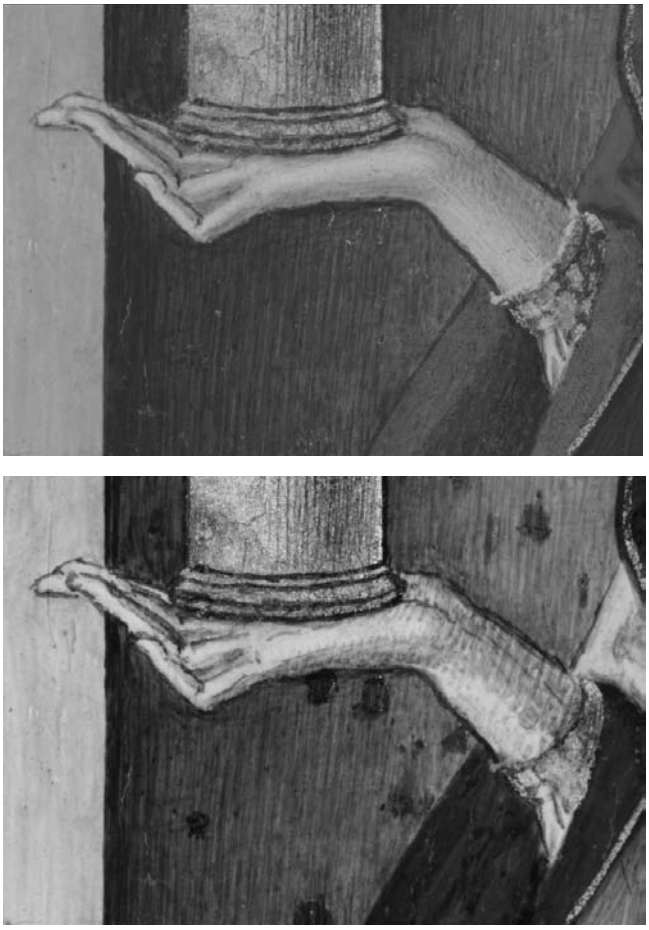

Figure 16. A comparison of a 560 nm and a 900 nm image of a detail from NG 907.2: the infrared image clearly shows the underdrawing and the retouchings.

Conclusions

We have shown that the new multispectral system described in this article is capable of producing accurate spectral reflectance curves for paintings without any spectral reconstruction other than a simple interpolation to the data measured in the 13 channels from 400 to 1000 nm. The new multispectral system can be used like a low resolution spectrophotometer where only standard calibrations such as dark subtraction, white balancing and flat-fielding are need. There is no need to use color calibration charts for spectral or colorimetric reconstruction. Only a small Macbeth chart is needed for quality control.

We have also demonstrated that with the addition of information from the near infrared, the multispectral system has some promise as a non-destructive and non-invasive method for pigment identification. The method is unlikely to replace other methods of examination, particularly microscopic examination of the surface; at present, pigment identification requires additional clarifying or corroborating information from other techniques. However, pigment identification will become more secure as more reference pigments are measured with the multispectral system and, as in this study, recorded spectra are correlated to pigment mixtures by examining the composition using microscopy or analytical methods. The multispectral images are also useful for identifying areas of retouching and revealing underdrawing. Finally, the multispectral images would form a useful database for 'spectral' printing.

Acknowledgment. We would like to thank Mohamed Benchouika for measuring the CCD response, Marika Spring and Ashok Roy for examining and photographing the paint samples from St Mary Magdalene, Boris Pretzel for access to the Victoria and Albert Museum Hitachi U-4000 spectrophotometer, and Clare Richardson for preparing the pigment library samples. This study was partly conducted within the EUsupported CRISATEL project (IST1999-20163): discussions with partners in the CRISATEL consortium are gratefully acknowledged.

References

1. K. Martinez, J. Cupitt and D. Saunders, "High Resolution Colorimetic Imaging of Paintings", *Proc. SPIE* **1901,** 25 (1993).
2. D. Saunders, H. Chahine and J. Cupitt, "Long-term Colour Change Measurement: Some Results After Twenty Years", *National Gallery Technical Bulletin* **17,** 81 (1996).
3. K. Martinez, J. Cupitt, D. Saunders, and R. Pillay, "10 years of Art imaging research", *Proc. IEEE* **90**(1), 28 (2002).
4. R. S. Berns and F. H. Imai, "The use of multi-channel visible spectrum imaging for pigment identification", *ICOM Committee for Conservation, 13th Triennial Meeting*, (ICOM Committee for Conservation, Rio de Janeiro, Brazil, 2002) p. 217.

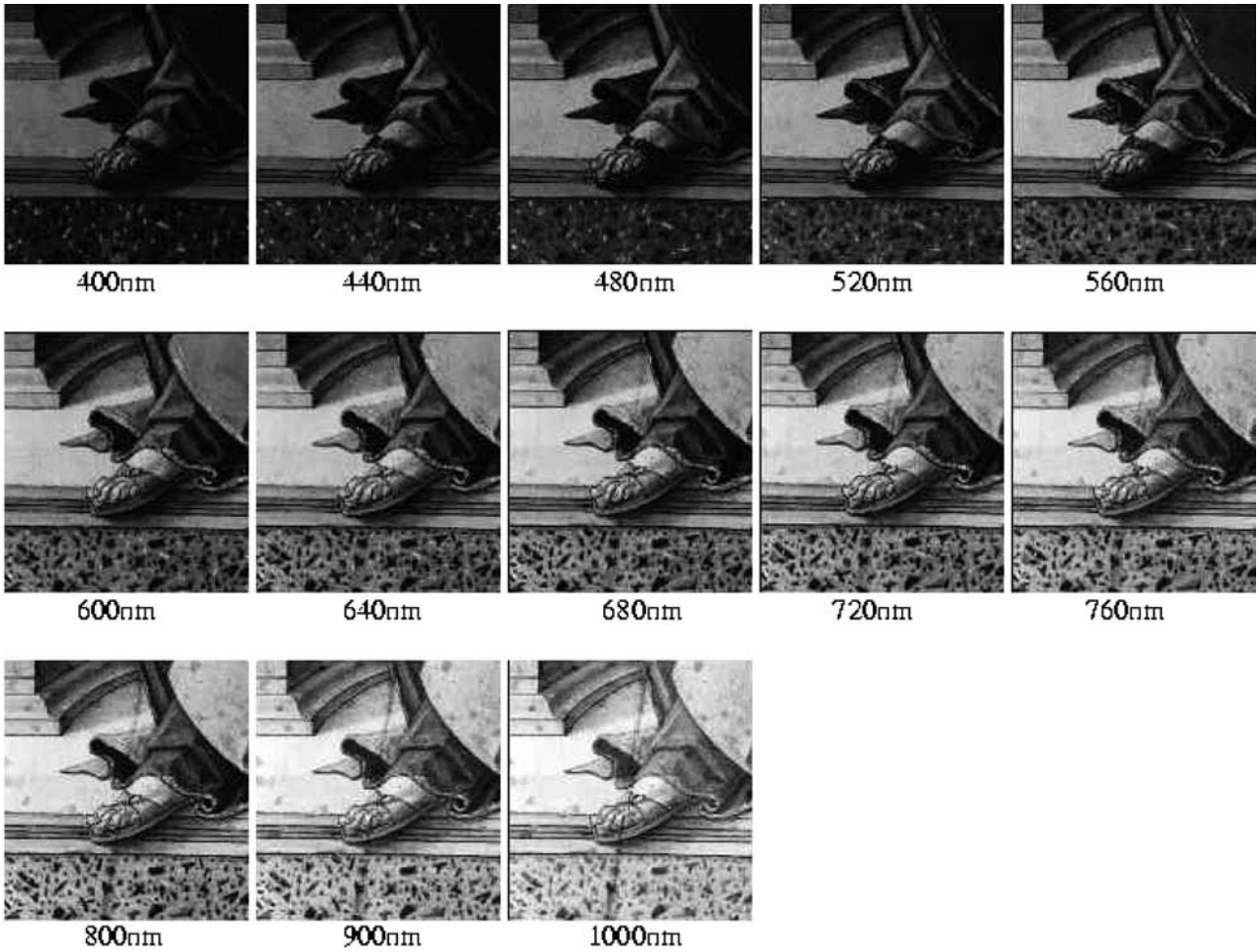

Figure 17. A set of multispectral images of a detail from NG 907.2.

5. C. Balas, V. Papadakis, N. Papadakis, A. Papadakis, E. Vazgiouraki, and G. Themelis, "A novel hyper-spectral imaging apparatus for the non-destructive analysis of objects of artistic and historic value", *J. Cultural Heritage* **4,** 330 (2003).
6. http://fors.ifac.cnr.it/index.php
7. C. Lahanier, G. Alquié, P. Cotte, C. Christodes, C. de Deyne, R. Pillay, D. Saunders, and F. Schmitt, "CRISATEL: A High Definition and Spectral Digitisation of Paintings with Simulation of Varnish Removal", (*ICOM Committee for Conservation, 13th Triennial Meeting*, ICOM Committee for Conservation, Rio de Janeiro, Brazil, 2002) p. 295.
8. A. Ribés, H. Brettel, F. Schmitt, H. Liang, J. Cupitt, and D. Saunders, "Color and Multispectral Imaging with the CRISATEL Multispectral System", *Proc. IS&T's PICS*, (IS&T, Springfield, VA, 2003) p. 215.
9. K. McLaren, "The development of the CIE 1976 (L*a*b*) uniform colour-space and colour-difference formula," *J. Soc. Dyers Colourists*, **92,** 338 (1976).
10. M. R. Luo, G. Cui and B. Rigg, "The Development of the CIE 2000 Colour-Difference Formula: CIEDE2000", *Color Res. Appl.* **26**(5), 340 (2001).
11. *CIE Colorimetry*, 3rd ed. CIE Publication 015:2004, (Central Bureau of the CIE, Vienna, 2004)
12. *CIE Technical Report: Improvement to Industrial Colour-difference Evaluation*, CIE Publication 142–2001, (Central Bureau of the CIE, Vienna, 2001)
13. J. Cupitt and K. Martinez, "VIPS: An Image Processing System for Large Images", *Proc. SPIE*, **1663,** 19 (1996).
14. J. Y. Hardeberg, "Filter Selection for Multispectral Color Image Acquisition", *Proc. IST's PICS*, (IS&T, Springfield, VA, 2003) p. 177.
15. R. Derby, "Applied Spectrophotometry. I. Color Matching with the Aid of the 'R' cam", *Amer. Dyestuff Reporter* **41,** 550 (1952).
16. P. Kubelka and F. Munk, "Ein Beitrag zur Optik der Farbanstriche", *Z. technische Physik* **12,** 593 (1931).
17. R. Berns, J. Kreuger and M. Swicklik, "Multiple Pigment Selection for Inpainting using Visible Reflectance Spectrophotometry", *Studies in Conservation* **47,** 46 (2002).
18. R. A. Lyon, *Technical Studies in the Field of the Fine Arts*, **2,** 203 (1933–1934).
19. M. Farnsworth, *Technical Studies in the Field of the Fine Arts*, **6,** 88 (1938–1939).